Freckle Formation and Freckle Criterion in Superalloy Castings

P. AUBURTIN, T. WANG, S.L. COCKCROFT, and A. MITCHELL

The evaluation of a numerical criterion to provide quantitative insight on freckling conditions is critical to the successful manufacture of large superalloy castings. Of the criteria reported in the literature, those based on the Rayleigh number seem best suited to predict the onset of freckle formation. However, in their current form, these criteria cannot explain why freckles develop predominantly at the surface of single crystal (SX) castings and at midradius in VAR/ESR ingots. An experimental Bridgman-type furnace has been built to directionally solidify freckle-prone superalloys, CMSX-11B, RENÉ88, NIM80A, WASPALOY, MAR-M247, and a variation of IN718 with high silicon content, at various angles to the vertical. Under typical industrial solidification conditions (thermal gradient between 500 and 4000 K m^{-1} ($5 < G < 40$ °C cm^{-1}) and solidification rate between 1.67×10^{-5} and 1.0×10^{-4} m s^{-1} ($1 < R < 6$mm min^{-1})), the results indicate a dependency of freckling on growth front angle likely related to the anisotropy in permeability. A modified Rayleigh criterion has been developed which accounts for directional permeability and orientation of the growth front relative to the gravity vector. Application to the experimental data shows good correlation with the onset of freckling for the range of solidification conditions examined in the study. The approximate threshold value for the modified Rayleigh number was estimated to be for CMSX-11B, 0.88, for RENÉ88, 0.90, for NIM80A, 0.85, for WASPALOY, 0.95, for MAR-M247, 0.86, and for IN718-Si, 0.65.

I. INTRODUCTION

A. *Background*

Freckles are a common defect found in nickel-based superalloy castings. They appear as a long trail of equiaxed grains with a composition shift consistent with alloy segregation. Some porosity and feeding shrinkage may also be present in and adjacent to the freckle line. Freckles are highly undesirable in critical applications because of their deleterious effect on mechanical performance. Moreover, castings containing freckles must be scrapped, causing considerable economic loss because they cannot be removed by postcast, thermomechanical treatments.

Development in large aircraft engines and also in large land-based gas turbines for power generation requires a considerable scale-up in the diameter of turbine disks and in the size of turbine blades. One of the main problems encountered in scaling-up has been the extensive freckling observed in these large castings, which has led to unacceptable rejection rates. Traditionally, for example, freckle formation in ingots can be avoided by keeping ingot diameters and melting rates below critical values, whereas in directional solidified (DS) and single crystal (SX) turbine blades, their occurrence has been avoided by maintaining high thermal gradients at the solidification front.

Two general approaches appear in the literature for predicting the onset of freckling: one, based on the use of mathematical criteria;[1–4] the other, based on solution of mass, momentum, energy, and species conservation equations.[5–10] While the latter approach is more fundamental, and may ultimately be applicable to a broader range of conditions, the computational severity of this approach together with the absence of high-temperature data presently precludes its practical application to industrial processes. Thus, given the present limitations, the best approach seems to be to adopt mathematical criteria for use with more straightforward "heat-flow" mathematical models.

B. *Literature Review*

It is now generally agreed that freckles arise due to channels associated with thermosolutal convection in the mushy zone and that they are driven by a variation in density originating from interdendritic segregation (Figure 1). A variety of straightforward mathematical criteria based on the local thermal gradient *G*, local solidification rate *R*, and local solidification time have been suggested in the literature.[1,3,11,12] Unfortunately, these simple criteria generally perform poorly against experimental results.[2] A mechanistically more correct criterion based on the Rayleigh number has also been suggested. The Rayleigh number represents the ratio of driving force for flow (in units of pressure per unit area) to resistance against flow (also in units of pressure per unit area) and, as such, may be employed to characterize the onset of fluid flow in unstable systems.[6,13]

While the basic mechanism of channeling as a precursor to freckling appears clear, there are differing views held as to where the channel actually nucleates in the mushy region. For example, Magirl and Incropera[14] and Sarazin and Hellawell[15] propose that the channels nucleate at the solid/liquid interface, at or near the liquidus temperature. Whereas, Fowler,[5] Worster,[6] and Tait and Jaupart[16] conclude that

P. AUBURTIN, formerly Postdoctoral Candidate, Department of Metals and Materials Engineering, University of British Columbia, is Process Modeling Research Engineer with PSA-Peugeot Citroen, Bievres, France 91570. T. WANG, Postdoctoral Candidate, S.L. COCKCROFT, Associate Professor, and A. MITCHELL, Professor, are with the Department of Metals and Materials Engineering, University of British Columbia, Canada V6T 1Z4.

Manuscript submitted August 23, 1999.

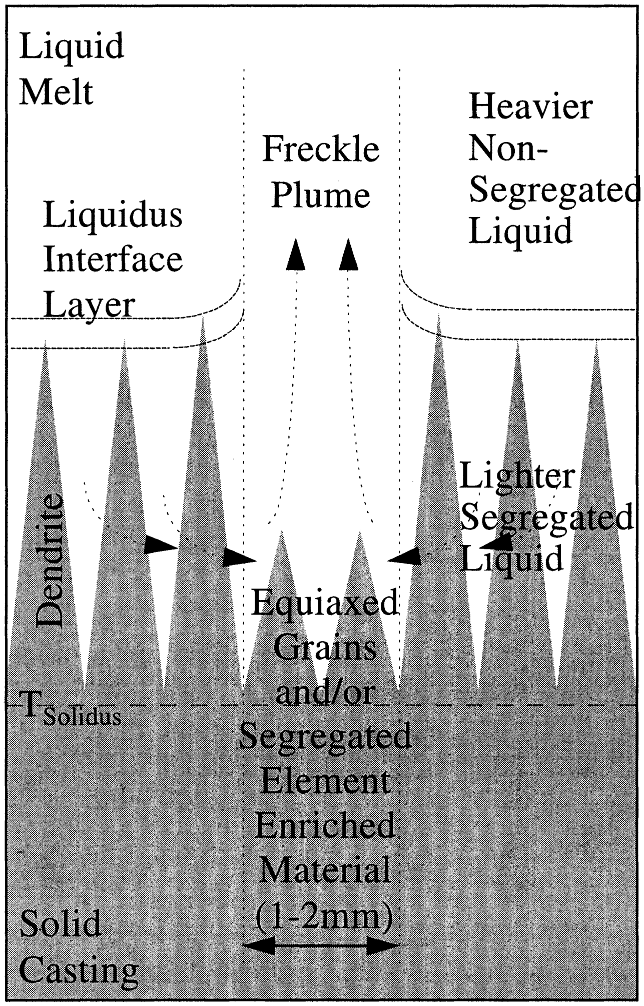

Fig. 1—Schematic illustration depicting freckle formation and associated fluid flow pattern.

the onset of convection and channels in the mushy zone is independent of boundary layer instabilities at the solid/liquid interface. And in yet another study, Auburtin *et al.*[17] have found that the channels appear to originate at a solid fraction of 0.5 in directionally cast superalloy samples.

The exact form of the Rayleigh number and the magnitude of the critical value for the onset of channeling also appear to be under debate. In their study on channeling in Pb-Sn and Pb-Sb alloys, Sarazin and Hellawell[15] employed the Rayleigh number of the form given in Eq. [1] to describe the onset of flow.

$$Ra = \frac{g \cdot \frac{d\rho}{dz}}{\frac{\eta D_T}{h^4}} \quad [1]$$

The parameters in Eq. [1] are defined in the Nomenclature list. By assuming a critical Rayleigh number of unity, they were able to back calculate the magnitude of the characteristic length scale, h, which was found to be on the order of the primary dendrite spacing λ_1. Other authors[6,16,18,19] have adopted a Rayleigh number of the form

$$Ra = \frac{g \Delta\rho K_0 h}{\eta D_T} \quad [2]$$

where K_0 is the representative flow permeability of the mushy zone. The characteristic length h has been assigned various values. For example, Tait and Jaupart[16] and Worster and Kerr[20] considered h as the thickness of the mushy zone. Whereas, Worster and Wettlaufer[21] and Lu and Chen[19] assumed h to be the thermal diffusion length $h = D_T/R$. Owing to variations in the characteristic length, the numerical value of the critical Rayleigh number in Eq. [2] is reported to vary in magnitude from 20 to several hundred.[22,23]

In addition to the uncertainties discussed, there are other troubling limitations with the basic Rayleigh number/criterion from a process application standpoint. For example, in vacuum arc remelting and electroslag remelting (VAR/ESR) ingots, freckles are found predominately at the midradius in ingots and not in the center where the Rayleigh number is at a maximum.[2] One possible explanation may lie in results of an early study conducted by Copley *et al.*[3] on the transparent analog system ammonium-chloride/water (NH_4Cl/H_2O). In their investigation, they found that in straightforward vertical solidification experiments, where the growth front was horizontal and flat, the freckles seemed to be randomly distributed across the casting. However, when the growth front was convex (higher at the center than the edges), the freckles appeared preferentially at the center. Alternatively, when the growth front was concave (higher at the edges than the center), freckles formed preferentially at the outside surface of the casting.

The importance of orientation on flow initiation in an unstable system is confirmed in another study conducted by Hart[13] aimed at investigating the evolution of convection patterns in water. In this investigation, Hart found that the onset of unstable convection was best described by the value of the Rayleigh number of the system and that the critical threshold value was dependent on the tilt angle of the experimental apparatus *via* the following relationship:

$$\text{Unstable flow for } Ra > Ra^* = 1708/\sin\alpha \quad [3]$$

Based on the literature reviewed, it is apparent that the Rayleigh number seems fundamentally correct as a criterion for predicting the onset of channeling leading to freckle formation in superalloy castings. However, it is unclear what temperature should be used for evaluation within the mushy regime (*i.e.*, at what fraction solidified), what the appropriate characteristic length should be, and what critical magnitude of Rayleigh number should be adopted as the criterion in superalloys. Moreover, it would appear that the basic criterion could benefit from incorporation of a dependency on growth front angle relative to the gravity vector.

In the present work, the influence of growth front angle on freckle formation in industrial superalloys is demonstrated in a series of experiments. Following this, a mechanism is proposed to explain the influence of growth front angle together with a modified, or alternative, Rayleigh number for superalloy casting processes. Employing the revised Rayleigh number, a characteristic length is set and critical values, Ra*, are estimated quantitatively for the experimental castings.

II. EXPERIMENTAL METHODOLOGY

Six industrial alloys were selected for this work: CMSX-11B,* RENÉ88,** NIM80A† WASPALOY,‡ MAR-M247,

*CMSX-11B is a trademark of Cannon-Muskegon Corp., Muskegon, MI.
**RENÉ88 is a trademark of General Electric Aircraft Engines, Fairfield, CT.
†Nim80A is a trademark of Inco Alloys International, Huntington, WV.
‡Waspaloy is a trademark of Pratt & Whitney, East Hartford, CT. Mar-M247 is a trademark of Martin-Marrietta Corp., Baltimore, MD. IN718 is a trademark of Inco Alloys International, Huntington, WV.

and IN718. All these alloys are nickel-based superalloys prone to freckle formation. The nominal compositions and melting range of these alloys can be found in Table I. The melting ranges of alloys CMSX-11B, NIM80A, and IN718 were determined by the Special Metal Corporation, New Hartford, NY. The melting range of alloy RENÉ88 was taken from Reference 24, and the melting range of WASPALOY and MAR-M247 were taken from Reference 25. In an attempt to induce upward channel flow in the IN718, pure Si was added to the commercially available IN718 alloy to make IN718-Si (freckles in IN718 have been reported to have a higher density than the alloy matrix and, therefore, form due to downward channel flow[26,27,28]). The chemistry of the IN718-Si tested is listed in Table II under "Matrix."

The tests were conducted in the Department of Metals and Materials Engineering, The University of British Columbia, in a vacuum induction furnace built in order to melt and directionally solidify 25-mm-diameter × 150-mm-long rods. The basic setup of the experimental apparatus is illustrated in Figure 2. It is similar to that of the classical Bridgman furnaces used in industry. Some of the features include an induction coil, graphite susceptor, water-cooled baffle and chill, and a variable speed withdrawal mechanism. The main feature of this furnace that differentiates it from its industrial counterparts is its ability to be tilted from 0 deg (conventional vertical operation) to 35 deg to the vertical.

To facilitate control and the recording of data relating to solidification, type-D tungsten-rhenium (W-3 pct Re/W-25 pct Re) thermocouples were used. All thermocouples were sheathed in 2-mm-diameter alumina tubing. The thermocouples were placed at various locations in the hot zone as well as inside the melt during calibration runs, as shown in Figure 2.

A typical casting procedure involved heating the furnace to the desired temperature, followed by a holding period to allow the sample to thermally equilibrate. The casting would then be withdrawn from the hot zone toward the cold zone at a prescribed rate. Further details on the furnace can be found in Reference 29.

Analysis of the thermocouple data revealed that except for short transient zones at the start and the end of solidification (bottom and top of the casting, respectively), the conditions prevailing at the growth front are relatively constant throughout the entire sample. The growth rate, R, in a steady-state operation, is dictated by the withdrawal rate, which can be adjusted by the operator between 1.67×10^{-5} and 1.0×10^{-4} m s^{-1} (1 and 6 mm min^{-1}). The thermal gradient at the growth front (G_L) could be adjusted between 500 and 4000 K m^{-1} (5 and 40 °C cm^{-1}) by manipulating the withdrawal rate and/or the temperature of the susceptor relative to the melting range of the alloy. The range of gradients and growth rates are typical of those commonly found in industry and result in a growth front that is essentially flat.

After completing a casting, the middle section of each sample (*i.e.*, steady-state solidification region) was visually inspected to determine whether freckles were present. The visual inspection was conducted on the as-cast and etched surface as well as etched cross sections of the rod. In the samples of WASPALOY, MAR-M247, CMSX-11B, and IN718-Si containing freckles, chemical analysis of the freckle trail was completed using an energy dispersion spectrometer (EDX) microprobe (KEVEX* detector and a Quartz XOne analyzer) attached to a Hitachi S-2300 scanning electron microscope (SEM). The procedure involved locating

*KEVEX is a trademark of Kevex Corporation, Foster City, CA.

Table I. Nominal Composition (in pct) and Melting Range of Cast Superalloys

Alloy	CMSX-11B	RENÉ 88	NIM80A	IN718*	WASPALOY	MAR-M247
T_S-T_L(K)	1548 to 1609	1523 to 1628	1586 to 1652	1526 to 1620	1603 to 1628	1553 to 1633
Ni	bal.	bal.	76.0	53.46	bal.	bal.
Co	7.0	13.0	—	0.2	12.3	10.0
Cr	12.5	16.0	19.5	18.12	19.0	8.5
Al	3.6	2.1	1.4	0.46	1.2	5.5
Ti	4.2	3.7	2.4	1.0	3.0	1.0
Hf	0.04	—	—	—	—	.4 1
Mo	0.5	4.0	—	2.96	3.8	0.6
Ta	5.0	—	—	—	—	.0 3
Nb	0.1	0.7	—	5.27	—	—
W	5.0	4.0	—	—	—	10.0
C	—	0.03	0.06	0.031	—	—
B	—	0.015	0.03	—	—	—
Mn	—	—	0.3	—	—	—
Si	—	—	0.3	0.08	—	—
Zr	—	—	0.06	—	—	—
Fe	—	—	—	18.24	—	—

*The tested alloy IN718-Si was made by adding 0.5 pct Si into IN718 alloy, with the resulting composition, as shown in Table II under "Matrix."

Table II. **Chemical Analysis of the Matrix and Freckles Found in Experimental Castings**

Alloy	WASPALOY Matrix (Wt Pct)	WASPALOY Freckle (Wt Pct)	MAR-M247 Matrix (Wt Pct)	MAR-M247 Freckle (Wt Pct)	CMSX-11B Matrix (Wt Pct)	CMSX-11B Freckle (Wt Pct)	IN718-Si Matrix (Wt Pct)	IN718-Si Freckle (Wt Pct)
Ni	56.89	56.96	57.42	56.58	59.02	61.75	53.41	51.88
Co	13.90	13.30	10.35	9.79	5.51	4.49	—	—
Cr	19.95	19.04	8.30	8.25	11.34	5.59	18.58	16.08
Al	1.64	1.59	5.79	5.91	2.93	3.32	0.38	0.33
Ti	3.03	4.12	0.78	1.01	3.93	7.08	0.90	1.39
Hf	—	—	1.73	2.71	0.16	0.22	—	—
Mo	4.59	4.99	0.62	0.76	0.48	0.26	2.86	3.79
Ta	—	—	4.08	5.16	6.23	9.40	—	—
Nb	—	—	—	—	0.13	0.11	4.05	8.86
W	—	—	10.93	9.83	9.90	7.77	—	—
Si	—	—	—	—	—	—	0.62	1.35
Fe	—	—	—	—	—	—	19.45	16.33

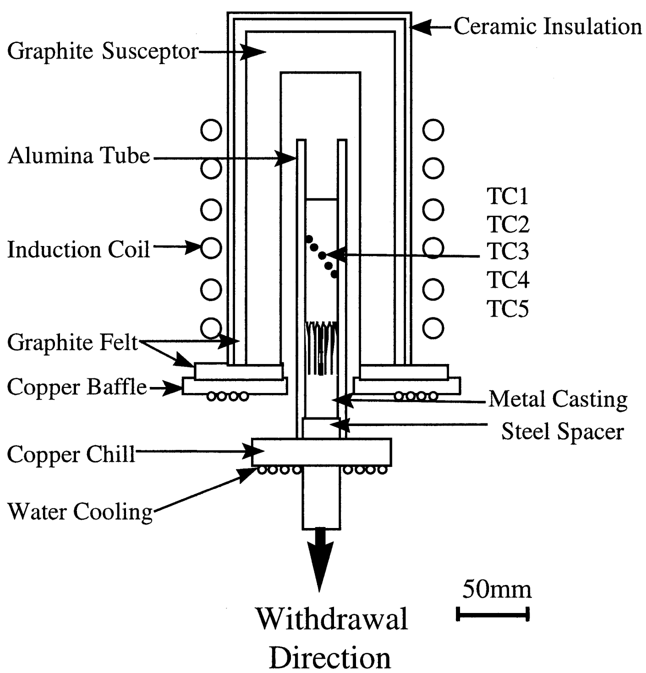

Fig. 2—Schematic diagram of the Bridgman-type furnace used in this study and the locations of thermocouples TC1, TC2, TC3, TC4, and TC5 used during the calibration of the PROCAST model.

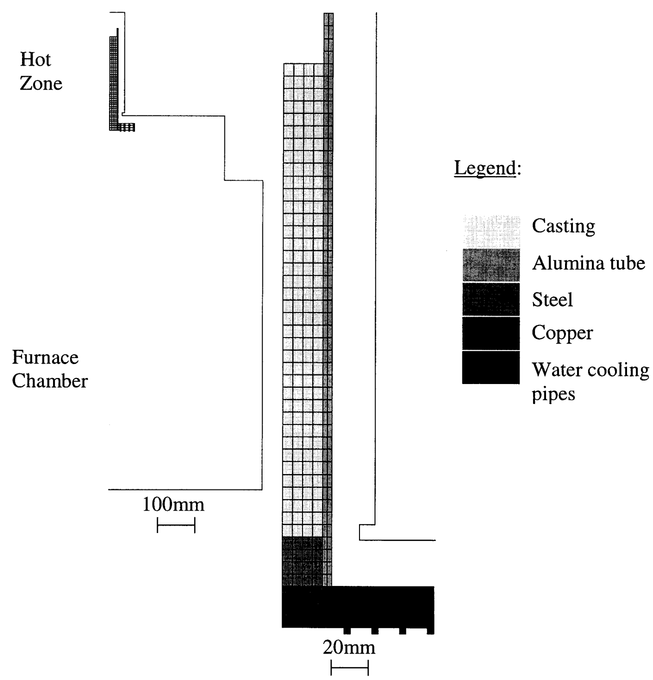

(a) Entire furnace. (b) Detail of the hot zone.

Fig. 3—Axisymetric mesh geometry used in PROCAST to model the experimental furnace.

freckle sites first at the etched cross section of samples by the darker appearance of freckles than the matrix. The freckle sites were then marked on the polished surface for SEM analysis.

Because the thermocouple data provides an incomplete picture of the solidification conditions prevailing at the growth front, the furnace was also modeled using the commercial finite element (FE) package ProCAST*. The model used the physical properties of IN718, as is common practice,[10] and was calibrated against thermocouple measurements at various locations within the sample taken under a variety of operating conditions (*i.e.*, withdrawal rate and susceptor temperature). The FE mesh used in the analysis is shown in Figure 3. The model included the casting, alumina tube (mold), steel spacer, water-cooling tubes, and furnace enclosure. The furnace enclosure was modeled to permit radiation view factors to be updated as the casting is withdrawn from the hot zone. Figure 4 schematically illustrates the various boundary conditions applied in the model. The values adopted for the various interfacial heat transfer coefficients, material emissivities, and temperature constraints are presented in Table III together with the initial conditions for the various materials. To simulate the casting process, the model is run for a period of time with the casting stationary until thermal equilibrium is reached. In this manner, the initial temperature distribution in the casting and furnace components is determined prior to commencing withdrawal of the ingot.

Overall, the model was able to reproduce the observed temperature variation satisfactorily with deviations of less

*ProCAST is a trademark of UES Inc., Dayton, OH.

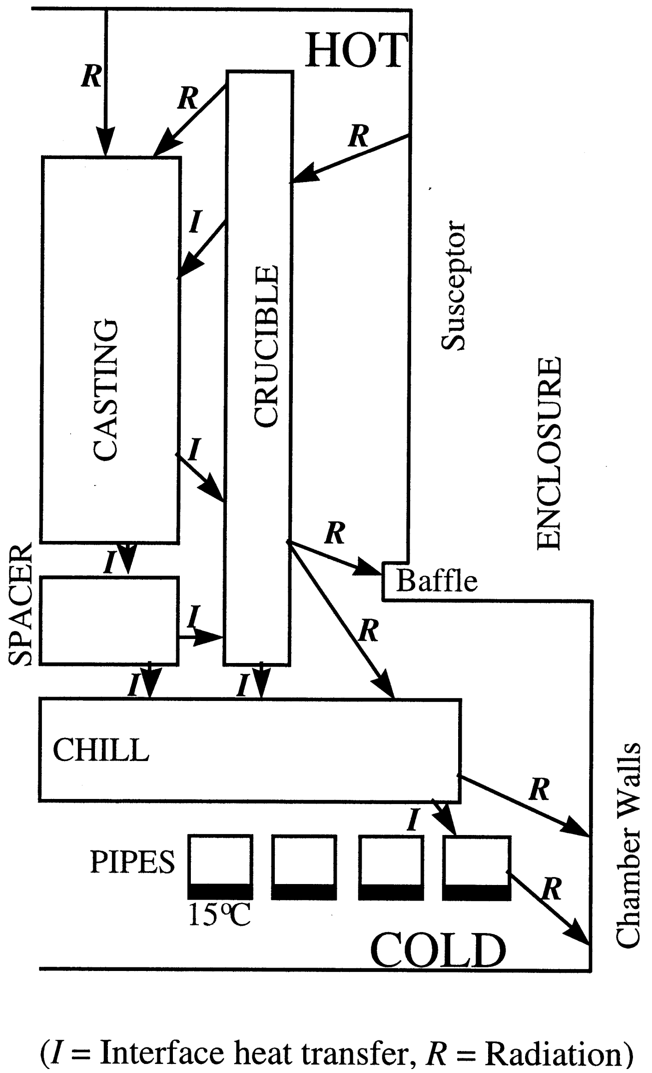

Fig. 4—Schematic heat flow diagram in the PROCAST model of the experimental tiltable furnace.

than 15 K throughout the solidification range, which is comparable to the estimated precision of the thermocouple measurements. A typical comparison between the thermocouple measurements and the predicted temperatures is shown in Figure 5. In Figure 5, the thermocouple data appear as the dark lines, and the model predictions appear as the lighter lines. Additional details on the model and its calibration can be found in Reference 29.

III. RESULTS AND DISCUSSION

A. *Analysis of Experimental Results*

Longitudinal sections of typical castings solidified at angles of 0 and 35 deg to the vertical are shown in Figure 6. The initial liquidus isotherm (melt limit of charge) is identified by the dashed lines appearing on the photomicrographs. For the 0 deg sample, the liquidus isotherm is initially flat and perpendicular to the long axis of the casting. The grains have grown parallel to the long axis of the casting in alignment with the direction of heat flow. In the sample solidified at 35 deg, there is some curvature likely due to convection in the melt that develops during the holding delay prior to commencing the withdrawal. It is also apparent that there was some vertical grain growth initially. However, after a short distance, the grains become aligned with the direction of heat flow. Thus, in the steady-state growth regime, it is possible to conclude that the growth front is approximately perpendicular to the long axis of the casting independent of furnace angle. Furthermore, if that holds, then the tilt angle of the furnace is representative of the angle of the growth front relative to the vertical or gravity vector.

The typical appearance of freckles in a casting is shown in Figure 7. It can be seen that freckles appear on the surface of the sample, similar to what has been observed by Giamei and Kear.[30] The results of a typical microprobe analysis of the freckles are presented in Table II and indicate segregation of alloy constituents. The amount of the shift in composition is similar to that found in freckles in industrial castings,[29] confirming that the segregates in the experimental samples are indeed freckles.

B. *Application of the Conventional Rayleigh Criterion*

Because of the uncertainty over choosing an appropriate characteristic length, it seems reasonable to adopt the approach suggested by Sarazin and Hellawell[15] of setting $h = \lambda_1$, which should yield Rayleigh numbers around 1. For the sake of convenience, the original Rayleigh number from Eq. [1] has been rearranged to the form given in Eq. [4].

$$Ra = 4.16 \times 10^{-6}\, G_F^V\, (G_L\, R)^{-1.32} \quad [4]$$

This manipulation has been accomplished as follows: first, the expression for the gradient in density in Eq. [1] has been replaced by

$$\frac{d\rho}{dz} = \frac{d\rho}{dT} \times \frac{dT}{dz} = \frac{d\rho}{dT} G_F^V \quad [5]$$

where G_F^V represents the vertical temperature gradient (*i.e.*, the gradient parallel to the gravity vector at the freckle initiation temperature).

Second, the characteristic length, h, set equal to the primary dendrite arm spacing λ_1, has been evaluated according to the following expression:[31,32]

$$\lambda_1 = \frac{150 \times 10^{-6}}{(G_L\, R)^{0.33}} \quad [6]$$

where λ_1 is in meters, and the cooling rate $G_L \times R$ is in K s^{-1} (where R is the solidification rate, and G_L is the temperature gradient at the liquidus). Finally, the remaining terms, g, $d\rho/dT$, η, and D_T have been evaluated as given subsequently and have been lumped into a single proportionality constant independent of alloy:[2]

$$\frac{d\rho}{dT} = 30 \text{ (kg m}^{-3}\text{ K}^{-1}) \quad [7]$$

$$g = 9.81 \text{ (ms}^{-2}) \quad [8]$$

$$\eta = 0.004 \text{ (kg m}^{-1}\text{ s}^{-1}) \quad [9]$$

$$D_T = 9 \times 10^{-6} \text{ (m}^2\text{ s}^{-1}) \quad [10]$$

In the present study, the freckle initiation temperature is assumed to be consistent with a fraction solidified $f_s = 0.5$, which is based on the results of a previous study.[17,29] The

Table III. Various Parameters Used in the PROCAST Model

Parameter	Location	Values
Heat transfer coefficient (W m^{-2} K^{-1})	chill / pipes	1500
	chill / spacer	150
	chill / alumina tube	30
	spacer / alumina tube	75
	spacer / casting	200
	casting / crucible (at solidus)	50
	casting / crucible (at liquidus)	500
Emissivities(—)	copper (baffle, chill)	0.3
	chamber walls	0.1
	alumina tube	0.4
	superalloy casting	0.4
	graphite	0.9
Temperature assigned to enclosure (K)	baffle top	1073
	baffle side	573
	chamber walls	373
	water pipes	288
Initial temperature (K)	superalloy casting	T_L of the superalloy
	alumina tube	T_L of the superalloy
	steel spacer	873
	water cooled copper chill	288

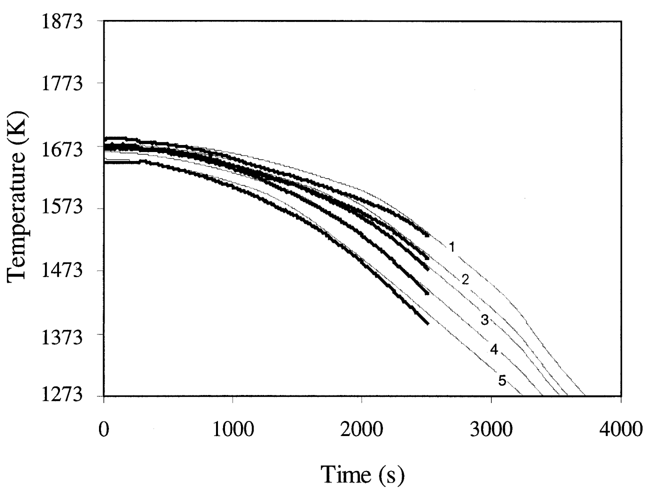

Fig. 5—Comparison between measured (bold lines) and predicted (thin lines) thermal history at five locations inside the casting (130, 122, 117, 110, and 100 mm above the top of the chill; see TC1, TC2, TC3, TC4, and TC5 in Fig. 3). (Control temperature: 1708 K; withdrawal rate: 3.3 × 10^{-5} ms^{-1}).

term $d\rho/dT$ is a function of both thermal and solute effects and has been estimated using the code METALS provided by the National Physical Laboratories UK (NPL). The procedure involves input of the measured freckle composition and is outlined in Reference 29. The temperature gradient at the liquidus, G_L, solidification rate, R, at the liquidus as well as the temperature gradient at the fraction solidified for freckle initiation of 0.5, $G_{0.5}$, have been evaluated using ProCAST according to the methodology presented in the User's Manual. The vertical temperature gradient G_F^V is simply equal to $G_{0.5}$ cos α, where α is the growth front angle to the horizontal.

The rationale for evaluating a single proportionality constant for all of the alloys examined in the study is that their probable variation over the alloy range chosen is within the

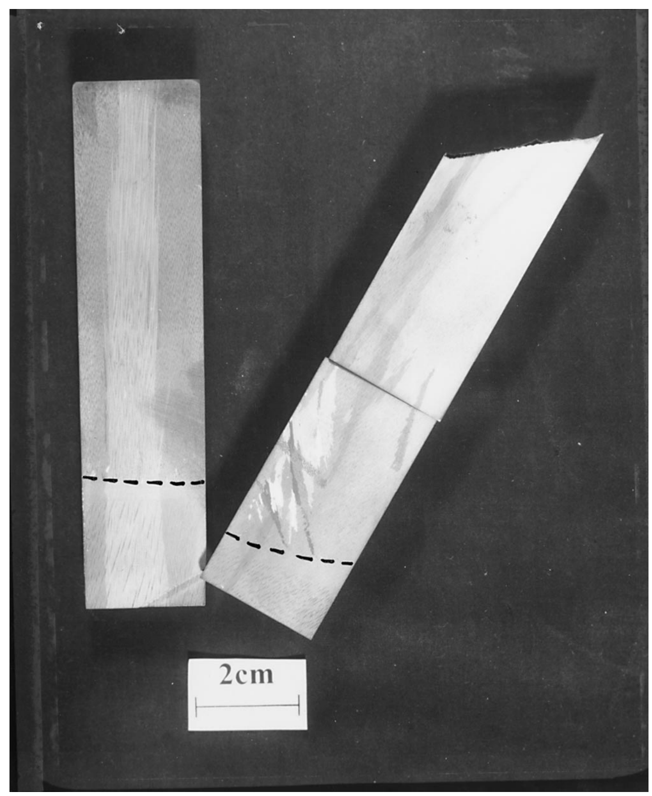

Fig. 6—Typical DS samples cast at 0 and 35 deg to the vertical.

experimental error of the determination of those particular properties at high temperature. Also, it permits a comparison between the various alloys on the basis of casting conditions only.

Having evaluated the Rayleigh number for all of the casting conditions examined, the results can be plotted as a function of furnace growth front angle for the six alloys. The resulting plot is presented in Figure 8. Given the range

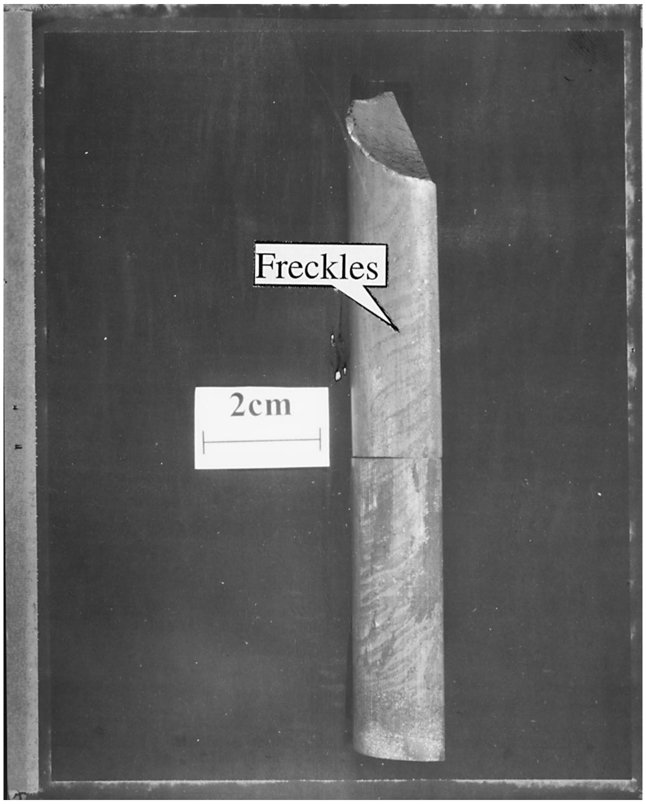

Fig. 7—Typical appearance of freckles on the etched surface of the DS samples.

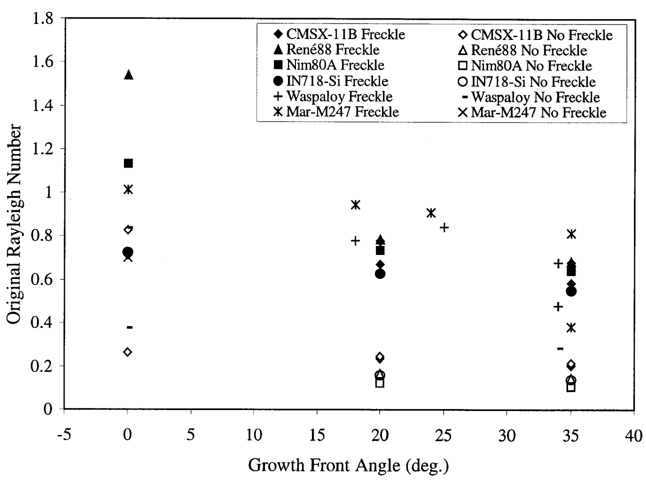

Fig. 8—Original Rayleigh number *vs* growth front angle for the experimental alloys.

of variation in thermal gradients and solidification rates observed in the quasi-steady-state sections of each sample, the Rayleigh numbers can be calculated with an estimated precision of approximately ± 15 pct.[29] As can be seen, except for alloys RENÉ88, NIM80A, and IN718-Si, which have only five experimental datum points for each alloy, it is not possible to draw a line horizontally that delineates a single value for the Rayleigh number above which no freckling occurs and below which freckling occurs. Therefore, either the basic Rayleigh number as a criterion is incorrect or there is a dependency on growth front angle.

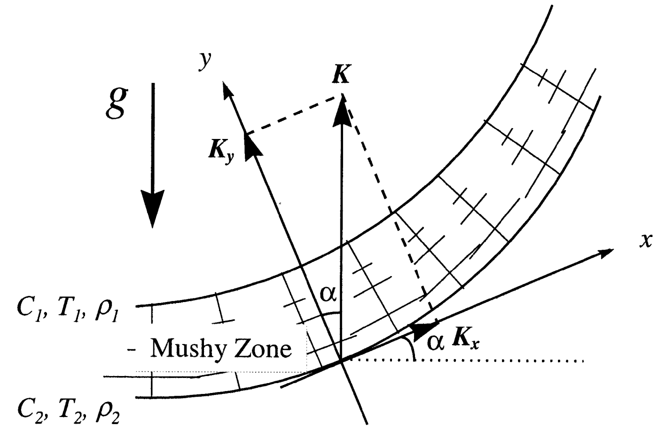

Fig. 9—Schematic illustration of typical curved growth front found in ingot.

C. *Modified Rayleigh Number*

In the original work of Sarazin and Hellawell,[15] the characteristic length for channeling in Pb-Sn and Pb-Sb alloys was determined by setting the Rayleigh number equal to unity, consistent with a balance between the driving force and resistance to flow. The fact that the characteristic length, h, determined in this manner was roughly consistent with the primary dendrite arm spacing may have been somewhat fortuitous or alternatively may indicate the influence of primary dendrite arm spacing on buoyancy boundary layer stability. In other studies, the characteristic length term has been rewritten to include the permeability of the medium in which liquid convection occurs. Both approaches have their merits since physical reasoning demands that the magnitude of the Rayleigh number should be around unity if a "balance" does indeed exist. Moreover, the characteristic length should include the permeability as it appears in the denominator in the Rayleigh number, contributing to the resistance to flow. The potential role of permeability can be illustrated by considering a schematic illustration of a typical mushy zone arising in an ingot cast *via* an ESR or VAR process (refer to Figure 9). It is obvious that at the center of the ingot (left-hand side of Figure 9, vertical channeling would be expected to see a "characteristic length" consistent with flow in a direction parallel to the primary dendrites. Whereas vertical channeling occurring toward the ingot surface, on the right-hand side of Figure 9, would be expected to see a "characteristic length" consistent with flow more perpendicular to the primary dendrite trunks.

Based on the previously mentioned arguments, a modified characteristic length of the form presented in Eq. [11] has been proposed as

$$h = \lambda_1 \left(\frac{K}{K_y}\right) \qquad [11]$$

where K is the permeability in the vertical direction, and K_y is the permeability parallel to the primary dendrite trunk. Poirier and co-workers[33,34] have developed the following expressions for permeability perpendicular and parallel to the primary dendrites:

$$K_y = 3.75 \times 10^{-4} f_L^2 \lambda_1^2 \quad \text{for } 0.17 < f_L < 0.61 \qquad [12]$$

$$K_x = 3.62 \times 10^3 f_L^{3.34} \lambda_1^{0.699} \lambda_2^{2.73} \text{ for } 0.19 < f_L < 0.66 \qquad [13]$$

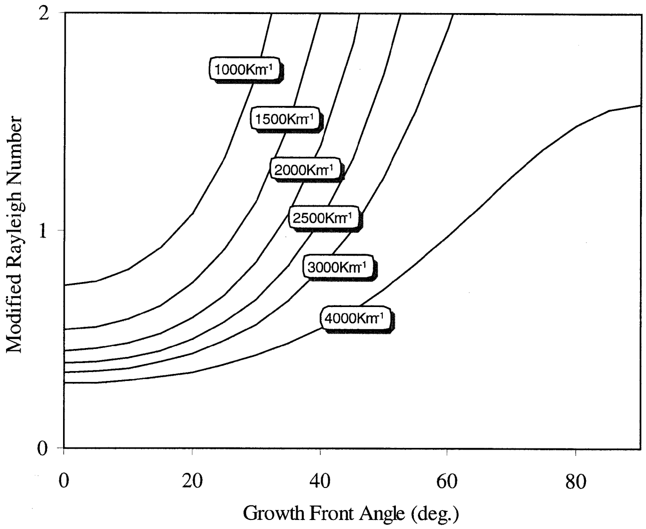

Fig. 10—Modified Rayleigh number *Ra vs* growth front angle for various thermal gradients G_L and $G_F^V = G_L + 1000$ K m^{-1} (constant growth rate $R = 3.3 \times 10^{-5}$ ms^{-1} (2 mm min^{-1})).

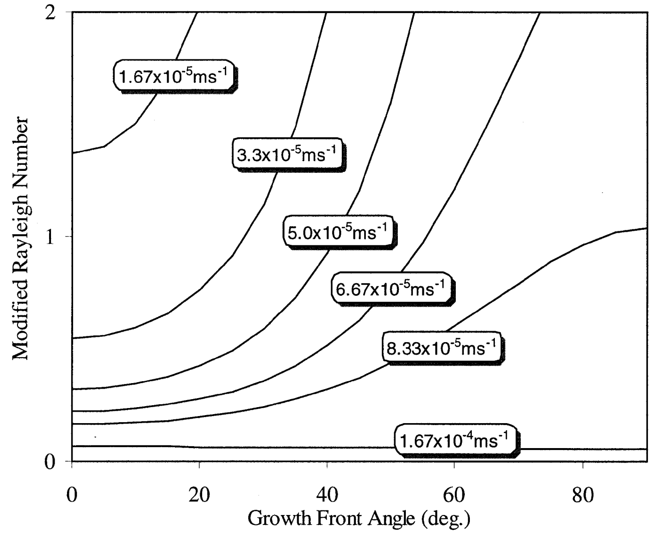

Fig. 11—Modified Rayleigh number *Ra vs* growth front angle for various growth rates *R* (constant thermal gradients G_L = 1500 K m^{-1} and G_F^V = 2500 K m^{-1}).

where λ_1 and λ_2 are in meters, and K_x and K_y are in square meters.

According to Scheideger,[35] the permeability in the vertical direction is given by the expression

$$K = \frac{1}{\dfrac{\sin^2\alpha}{K_x} + \dfrac{\cos^2\alpha}{K_y}} \qquad [14]$$

In Eqs. [12] and [13], λ_1 is the primary dendrite arm spacing, λ_2 is the secondary dendrite arm spacing, and f_L is the liquid fraction; the rest of the parameters are defined in the nomenclature list at the end of the article. In the present study, λ_1 is evaluated according to Eq. [6] given previously, and λ_2 is evaluated according to Eq. [15] given[31,32] as

$$\lambda_2 = \frac{40 \times 10^{-6}}{(G_L R)^{0.42}} \qquad [15]$$

where λ_2 is in meters $G_L R$ is in K s^{-1}.

For the structure on the left-hand side of Figure 9, Eq. [11] yields λ_1 because K will be equal to K_y, resulting in a Rayleigh number close to unity in agreement with Sarazin and Hellawell.[15] For the structure on the right-hand side, K is increased reflecting the influence of the perpendicular component of permeability, which is between 2 and 4 times greater than the parallel component at f_L =0.5.

Employing the revised expression for characteristic length, a modified Rayleigh number can, therefore, be written as

$$\text{Ra} = \frac{gd\rho\,/\,dz}{\eta D_T}\left[\lambda_1\left(\frac{K}{K_y}\right)\right]^4 \qquad [16]$$

To illustrate the effect of variation in growth front angle on *Ra*, the modified Rayleigh number has been plotted against growth front angle α for a variety of different solidification conditions. The results for different gradients, at a constant growth rate, appear in Figure 10, and the results for different growth rates, at a constant gradient, appear in Figure 11. As can be seen, under typical industry conditions ($R < 1.67 \times 10^{-4}$ ms^{-1} (6 mm min^{-1})), the Rayleigh number increases with the solidification front angle.

D. *Application of Modified Rayleigh Criterion to the Experimental Results*

In the general case of ingot casting, the mushy zone and the corresponding isotherms are curved as illustrated in Figure 9, such that at a given location the tangent to a particular isotherm forms an angle α with the horizontal. The grains growing perpendicular to the isotherms will form the same angle α with the vertical. This growth geometry is also consistent with the experimental samples produced in this study.

To assess the applicability of the proposed modifications, the experimental results were reexamined, and new Rayleigh numbers have been calculated for each casting. Once the necessary numerical data has been incorporated into the expression for the modified Rayleigh number, the relationship may be simplified to the following form:

$$\text{Ra} = 4.14 \times 10^{-6}\, G_F^V\,(G_L\,R)^{-1.32}\left(\frac{K}{K_y}\right)^4 (\pm 15 \text{ pct}) \qquad [17]$$

In Eq. [17], the values for the viscosity, diffusivity, permeability, and gradient in density with temperature are the same as those used previously and are given by Eqs. [7] through [10] and [12] through [14]. The appropriate values for *G* and *R* for each casting have been obtained from ProCAST as before. For each experimental casting, the Rayleigh number Ra has been plotted against growth front angle. The results are presented in Figures 12(a) through (d) together with a line delineating the freckled and freckle-free regions. As can be seen, in all cases, it is now possible to evaluate for each alloy a critical threshold value Ra* independent of growth front angle, below which freckling does not occur and above which freckling occurs. Accordingly, estimates from the present experimental results are

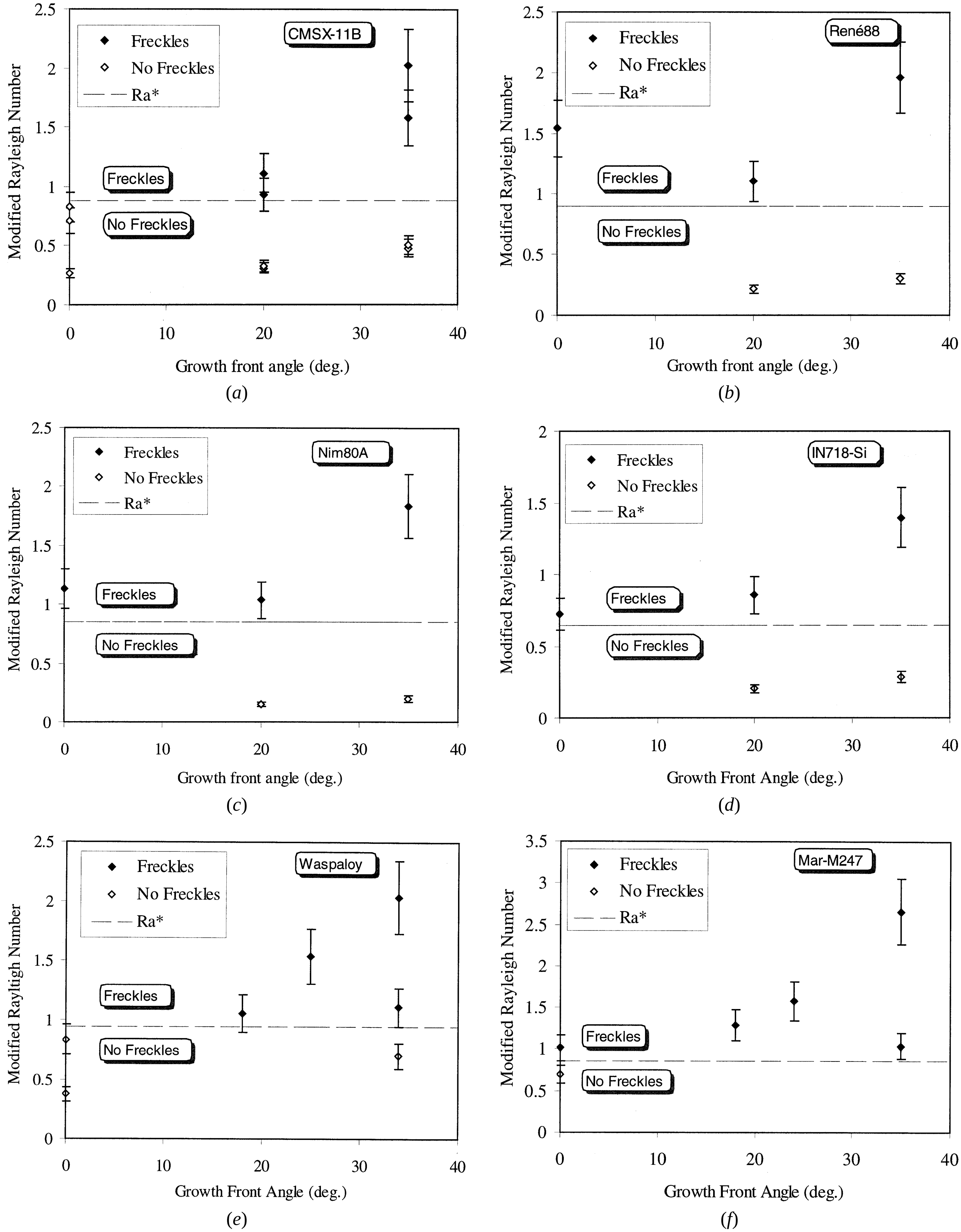

Fig. 12—Modified Rayleigh number *vs* growth front angle for alloy:(*a*) CMSX-11B, (*b*) RENÉ88, (*c*) NIM80A, (*d*) IN718-Si, (*e*) WASPALOY, and (*f*) MAR-M247.

$$Ra^*(\text{CMSX-11B}) \approx 0.88$$

$$Ra^*(\text{RENÉ88}) \approx 0.90$$

$$Ra^*(\text{NIM80A}) \approx 0.85$$

$$Ra^*(\text{IN718-Si}) \approx 0.65$$

$$Ra^*(\text{WASPALOY}) \approx 0.95$$

$$Ra^*(\text{MAR-M247}) \approx 0.86$$

It can be seen that the critical threshold values *Ra** are very similar for all alloys and are close to unity. It is to be recalled that the analysis uses proportionality coefficients, and, hence, the actual threshold values may be slightly different. However, if the results of the present study are assumed to be indicative of the relative propensity of each alloy to form freckles, then WASPALOY appears to be less freckle-prone because it has the higher critical threshold value Ra*, whereas IN718-Si is the most prone to freckle formation.

IV. SUMMARY AND CONCLUSIONS

Freckles are presently one of the major defects encountered in large superalloy castings. The evaluation of a numerical criterion able to provide quantitative insight on the conditions of freckle formation is now recognized as a major key toward the successful manufacture of large diameter VAR/ESR ingots and large DS/SX castings. An experimental furnace was built to directionally solidify cylindrical castings at various angles to the vertical, thus simulating a tilted mushy zone. Analysis of the results using the conventional Rayleigh number reveals no single criterion above which freckling occurs and below which no freckling occurs for the alloys examined in the study, CMSX-11B, RENÉ88, NIM80A, WASPALOY, MAR-M247, and a variation of IN718 with high silicon content.

Based on a review of the literature, a modified Rayleigh number has been proposed. The modified number uses a characteristic length that includes dendrite permeability and also accounts for its dependence on growth front angle and on the local solidification conditions. The modified Rayleigh number has been used to analyze the results of the experimental study. Using the modified number, a single threshold value can be determined in all cases. For CMSX-11B, the threshold value is approximately 0.88; for RENÉ88, it is approximately 0.90; for NIM80A, it is approximately 0.85; for WASPALOY, it is approximately 0.95; for MAR-M247, it is approximately 0.86; and for IN718-Si, it is approximately 0.65. The values are seen to be close to unity as is intuitively expected from the physical basis of Ra.

Overall, the results of the study clearly demonstrate the influence of growth front angle on channel formation as it was found that, under similar solidification conditions, tilted castings exhibited freckles, whereas vertical castings were freckle-free. Subsequent analysis of the results with the modified Rayleigh criterion illustrates the efficacy of proposed criterion for industrial superalloy castings. In addition, practical threshold values for industrial superalloys have also been determined, which may be used to develop procedures for casting and remelting operations.

NOMENCLATURE

α	growth front angle (deg)
D_T	thermal diffusivity (m^2 s^{-1})
$\Delta\rho$	density difference (kg m^{-3})
$d\rho/dz$	density inversion term in vertical direction (kg m^{-4})
$d\rho/dT$	density inversion term (kg m^{-3} K^{-1})
f_L	fraction liquid
g	gravitational constant (m s^{-2})
$G_{0.5}$	temperature gradient at isotherm $f_L = 0.5$ (K m^{-1})
G_F^V	vertical temperature gradient at isotherm $f_L = 0.5$ (K m^{-1})
G_L	temperature gradient parallel to sample axis (K m^{-1})
η	dynamic viscosity (kg m^{-1} s^{-1})
h	characteristic length (m)
K	permeability in vertical direction (m^2)
K_0	representative permeability of mushy zone (m^2)
K_x	perpendicular permeability (m^2)
K_y	parallel permeability (m^2)
λ_1	primary dendrite arm spacing (m)
λ_2	secondary dendrite arm spacing (m)
R	solidification rate (m s^{-1})
Ra	Rayleigh number
Ra*	critical threshold value of Rayleigh number

REFERENCES

1. T.M. Pollock and W.H. Murphy: *Metall. Mater. Trans. A*, 1996, vol. 27A, pp. 1081-94.
2. P. Auburtin and A. Mitchell: *Liquid Metal Processing and Casting AVS Conf.*, Santa Fe, NM, American Vacuum Soc., NY, Feb. 1997, pp. 18-34.
3. S.M. Copley, A.F. Giamei, S.M. Johnson, and M.F. Hornbecker: *Metall. Trans.*, 1970, vol. 1, pp. 2193-2204.
4. J.R. Sarazin and A. Hellawell: in *Advances in Phase Transition*, J.D. Embury and G.R. Purdy, eds., Pergamon Press, Oxford, United Kingdom, 1988, pp. 101-15.
5. A.C. Fowler: *IMA J. Appl. Math.*, 1985, vol. 35, pp. 159-74.
6. M.G. Worster: *Ann. Rev. Fluid Mech.*, 1997, vol. 29, pp. 91-122.
7. J.C. Heinrich, S. Felicelli, and D.R. Poirier: *Num. Heat Transfer, Part B*, 1993, vol. 23, pp. 461-81.
8. W.D. Bennon and F.P. Incropera: *Num. Heat Transfer*, 1988, vol. 13, pp. 277-96.
9. H. Combeau and G. Lesoult: in *Modeling of Casting, Welding and Advanced Solidification Processes VI*, T.S. Piwonka, V. Voller, and L. Katgerman, eds., TMS, Warrendale, PA, 1993, pp. 201-08.
10. M.C. Schneider, J.P. Gu, C. Beckermann, W.J. Boettinger, and U.R. Kattner: *Metall. Mater. Trans. A*, 1997, vol. 28A, pp. 1517-31.
11. A.L. Purvis, C.R. Hanslits, and R.S. Diehm: *JOM*, 1994, vol. 46(1), pp. 38-41.
12. R. Mehrabian, M. Keane, and M.D. Flemings: *Metall. Trans.*, 1970, vol. 1, pp. 1209-20.
13. J.E. Hart: *J. Fluid Mech.*, 1971, vol. 47, pp. 547-76.
14. C.S. Magirl and F.P. Incropera: *Trans. ASME*, 1993, vol. 115, pp. 1036-43.
15. J.R. Sarazin and A. Hellawell: *Metall. Trans. A*, 1988, vol. 19A, pp. 1861-71.
16. S. Tait and C. Jaupart: *J. Geophys. Res.*, 1992, vol. 97(B5), pp. 6735-56.
17. P. Auburtin, S.L. Cockcroft, and A. Mitchell: *Superalloys 1996*, TMS-AIME, Warrendale, PA, 1996, pp. 443-50.
18. P.W. Emms and A.C. Fowler: *J. Fluid Mech.*, 1994, vol. 262, pp. 111-39.
19. J.W. Lu and F. Chen: *J. Cryst. Growth*, 1997, vol. 171, pp. 601-13.
20. M.G. Worster and R.C. Kerr: *J. Fluid Mech.*, 1994, vol. 269, pp. 23-44.
21. M.G. Worster and J.S. Wettlaufer: *J. Phys. Chem. B*, 1997, vol. 101, pp. 6132-36.
22. P.W. Emms: *J. Eng. Math.*, 1998, vol. 33, pp. 175-200.
23. C.F. Chen and F. Chen: *J. Fluid Mech.*, 1991, vol. 227, pp. 567-86.

24. S.T. Wlodek, M. Kelly, and D.A. Alden: *Superalloys 1996*, TMS-AIME, Warrendale, PA, 1996, pp. 129-36.
25. N.S. Stoloff: *ASM International Metals Handbook*, 10th ed., J.R. Davis, K.M. Mills, S.R. Lampman, T.B. Zorc, H.F. Lampman, G.M. Crankovic, A.W. Ronke, S.D. Henry, J.L. Daquila, J. Jakel, K.L. O'Keefe, R.L. Stedfield, L.A. Abel, R.T. Kiepura, P. Thomas and N.D. Wheaton eds.; ASM INTERNATIONAL, Materials Park, OH, 1990, pp. 950-80.
26. James H. Van Den Avyle, John A. Brooks, and Adam C. Powell: *JOM*, 1998, vol. 50(3), pp. 22-25 and 49.
27. P. Auburtin: Master's Thesis, University of British Columbia, Vancouver, BC, Canada, Aug. 1995.
28. T. Wang: Master's Thesis, University of British Columbia, Vancouver, BC, Canada, May 1999.
29. P. Auburtin: Ph.D. Thesis, University of British Columbia, Vancouver, BC, Canada, Aug. 1998.
30. A.F. Giamei and B.H. Kear: *Metall. Trans.*, 1970, vol. 1, pp. 2185-92.
31. G.K. Bouse and J.R. Mihalisin: *Superalloys, Supercomposites and Superceramics*, J.K. Tien and T. Caulfield, eds., Academic Press Inc., London, 1989, pp. 99-148.
32. W. Kurz and D.J. Fisher: *Fundamentals of Solidification*, TransTech Publications, Aedermannsdorf, Switzerland, 1992, pp. 86 and 123-25.
33. D.R. Poirier: *Metall. Trans. B*, 1987, vol. 18B, pp. 245-56.
34. M.S. Bhat, D.R. Poirier, and J.D. Heinrich: *Metall. Mater. Trans. B*, 1995, vol. 26B, pp. 1049-56.
35. A.E. Scheidegger: *The Physics of Flow through Porous Media*, 3rd ed., University of Toronto Press, Toronto, 1974, pp. 78-83.